Thèse de doctorat

NNT: 2020UPASA000

Propriétés catalytiques à l'échelle nanométrique sondées par diffraction des rayons X de surface et imagerie de diffraction cohérente.

Catalytic properties at the nanoscale probed by surface x-ray diffraction and coherent diffraction imaging

Thèse de doctorat de l'Université Paris-Saclay

École doctorale n° 000, dénomination et sigle
Spécialité de doctorat: Physique
Unité de recherche: voir annexe
Référent: : voir annexe

Thèse présentée et soutenue à ....., le .... 2023, par

David SIMONNE

Composition du jury

Prénom Nom Titre, Affiliation	Président/e
Prénom Nom Titre, Affiliation	Rapportrice
Prénom Nom Titre, Affiliation	Rapporteur
Prénom Nom Titre, Affiliation	Examinatrice
Prénom Nom Titre, Affiliation	Examinateur
Prénom Nom Titre, Affiliationt	Examinateur

Direction de la thèse

Alessandro Coati Dr., Synchrotron SOLEIL	Directeur
Andrea Resta Dr., Synchrotron SOLEIL	Codirecteur
Marie-Ingrid Richard Dr., CEA Grenoble	Coencadrante

Contents

List of Figures

List of Tables

Chapter 1

Introduction

(The Introduction chapter should contain background information as appropriate, plus definitions of all special and general terms. Your topic should be: clearly stated and defined; have a clear overall purpose; and have clear, relevant and coherent aims and objectives. It is also informative to give a brief description of the contents of the remaining chapters of the thesis. This alerts the reader and prepares them for the rest of the thesis.)

1.1 The oxidation of Ammonia

Ammonia oxidation is an essential catalytic reaction used in the production of artificial fertilizers and in environmental applications. In both cases, particular focus is on two products of the reaction, namely, NO and N_2 . The selectivity toward either one is dictated by reaction parameters, that is, by temperature, NH_3 and O_2 partial pressures, and the type of catalyst.

Detail and literature about the oxidation of Ammonia on Platinum nano-catalyst can be found here (Resta et al. 2020).

1.1.1 From industry to model catalysis

"A long standing conundrum in the catalysis community emerged at the interface between surface science and heterogeneous catalysis, better known as the pressure and materials gap."

Nature Catalysis editorial, 2018.

	Pressure	Material	Temperature
Industry	1-12 bar	Wires ($\varnothing \approx 80\,\mu m$)	>1000 K
Literature	UHV, mbar	Single crystals	RT - 1000 K
This study	Near ambient pressure (0.5 bar)	Single crystals and nanoparticles	≈ 750 K

Table 1.1: Material and pressure gap in heterogenous catalysis.

1.1.2 Crystal structures

1.1.3 Pt 111

1.1.4 Pt 100

1.1.5 Nanoparticles

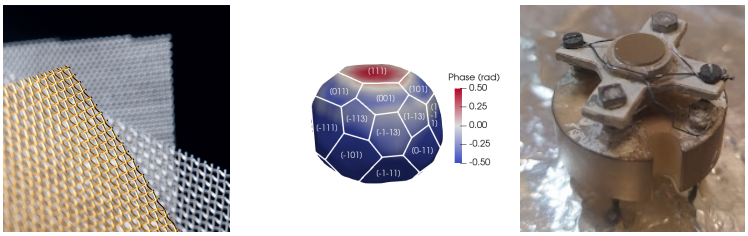

Figure 1.1: Platinum gazes used in industry (left), Pt particle measured at SixS, ⌀ is of about 300 nm (middle), Pt 111 single crystal used in SXRD and XPS experiments, ⌀ is of about 8 mm (right).

1.2 Aim and Scope

1.3 Outline of the Thesis

In the first chapter of this thesis we will come back to the basics behind each X-ray technique that was used to study the catalyst, as well as define the exact meaning of heterogeneous catalysis and how

In the second chapter we will present and discuss the results that we obtained with three different techniques

Chapter 2

Theory and methods

2.1 X-ray interaction with matter

Understanding the different mechanism at play when photons interact with matter is of crucial importance to be able to decide how to use X-rays as a probe in material science. Each phenomena is at the source of different techniques, diffraction brings surface X-ray diffraction (SXRD) and Bragg coherent diffraction imaging (BCDI), two techniques used in the frame of this thesis that give complementary information about the sample structure bulk and surface.

X-ray absorption together with the photoelectric effect explained by Einstein in 1905 are at the source of a third technique used, X-ray photoelectron spectroscopy, which yields information specific to the nature of the adsorbates on the sample's surface.

Technique	Sample	Sensitivity	Information
Bragg Coherent Diffraction Imaging (BCDI)	Pt nanoparticles (111), (110), (100), ...	Bragg electronic density	Shape, 3D strain and displacement arrays
Surface X-ray Diffraction (SXRD)	Pt single crystals (111), (100), (311)	Surface structure	Roughness, relaxation and crystallographic phases
X-ray Photoelectron Spectroscopy (XPS)	Pt single crystals (111), (100)	Surface species	Species presence, quantity, oxidation state

Table 2.1: Near-ambient pressure (NAP) X-ray techniques carried out at the SixS (SOLEIL) or B-07 (Diamond) beamlines

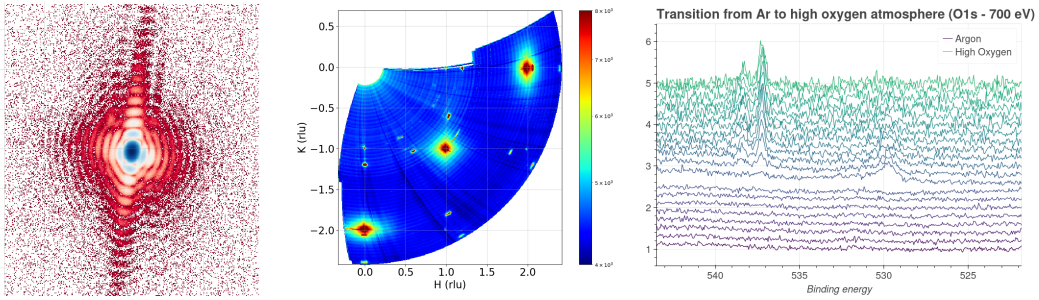

Figure 2.1: Slice of 3D diffraction pattern collected at the SixS beamline at the SOLEIL synchrotron (left). Reciprocal space map in HK plane collected at the SixS beamline at the SOLEIL synchrotron (middle). Ambient pressure XPS spectra collected during a transition between two atmospheres, collected at the B07 beamline at the Diamond synchrotron (right).

In this chapter we will discuss the origin of each technique from fundamentals that not only tailor their experimental design but also their operability and sensitivity.

2.1.1 Scattering from electrons and atoms

The duality between wave and particles was first mentionned by Max Planck and Albert Einstein in the early 20th century and generalized to all matter by Louis-Victor de Broglie in 1924 with the famous formula:

$$\lambda = \frac{h}{p} \tag{2.1}$$

Electromagnetic waves, i.e. light or photons can be characterized by their energy E in eV and wavelength λ in m. The conversion between is realized thanks to Planck's constant $h = 6.626 \times 10^{-34}$ J s and the speed of light in vacuum $c = 2.9979 \times 10^{8}$ m s^{-1} (eq. 2.2).

$$E = \frac{hc}{\lambda} \tag{2.2}$$

The properties of the photon and its use in our society depends on its energy and wavelength. If visible light is situated between 500eV and 900eV, micro-waves used in our everyday life are situated between 10^{-6}eV and 10^{-4}eV. On the other side of the electromagnetic spectrum, we have higher energy photons such as X-rays ($\in [10^2, 10^6]$eV) and γ-rays (above 10^{-6}eV).

X-rays have a wavelength of a few Å (10^{-10}m) making them the perfect probe to study the structures of materials at the atomic scale thanks to different interaction with matter.

Cross-sections

When an electromagnectic beam interacts with matter it will be attenuated by absorbtion, reflection or scattering. Each process can be quantified depending on the atoms (and thus on the electronic cloud) the beam interacts with and the energy on the incident photon, this is illustrated in figure 2.2. The cross-section for a particuliar process p is defined as follows (Willmott 2009):

$$\sigma_p = (\Lambda_p N_i)^{-1} \tag{2.3}$$

Λ_p is the attenuation length in m, i.e. the length after which the beam is reduced to $1/e$, N_i is the atomic number-density in atoms/unit volume.

Compton scattering, also named inelastic scattering, is a process during which some of the incident electromagnetic wave energy is transfered to the atoms' electrons. This results in a lower energy for the scattered photon (and therefore a higher wavelength) compared to the incident photon.

In the frame of this thesis, the (elastic) Thomson scattering cross-sections is the most important, at the origin of X-ray diffraction. This process is dominant for energies below 200keV, together with photoelectric absorption.

Scattering from an electron

We begin our discussion of X-ray scattering by considering scattering from a single free electron using classical electromagnetic theory. During elastic scattering, the oscillating electric field of the incident X-ray wave exerts an electromagnetic force on the electron, causing it to accelerate and oscillate in the same direction as the incident electronic field.

During an elastic scattering event, the oscillating electron emits a spherical electromagnetic wave with the same wavelength as the incident beam (Thomson scattering). The scattered field $\vec{E}_{scatt}$ is then proportional to the incident electromagnetic field $\vec{E}_{in}$ as follows (Jens Als-Nielsen 2011):

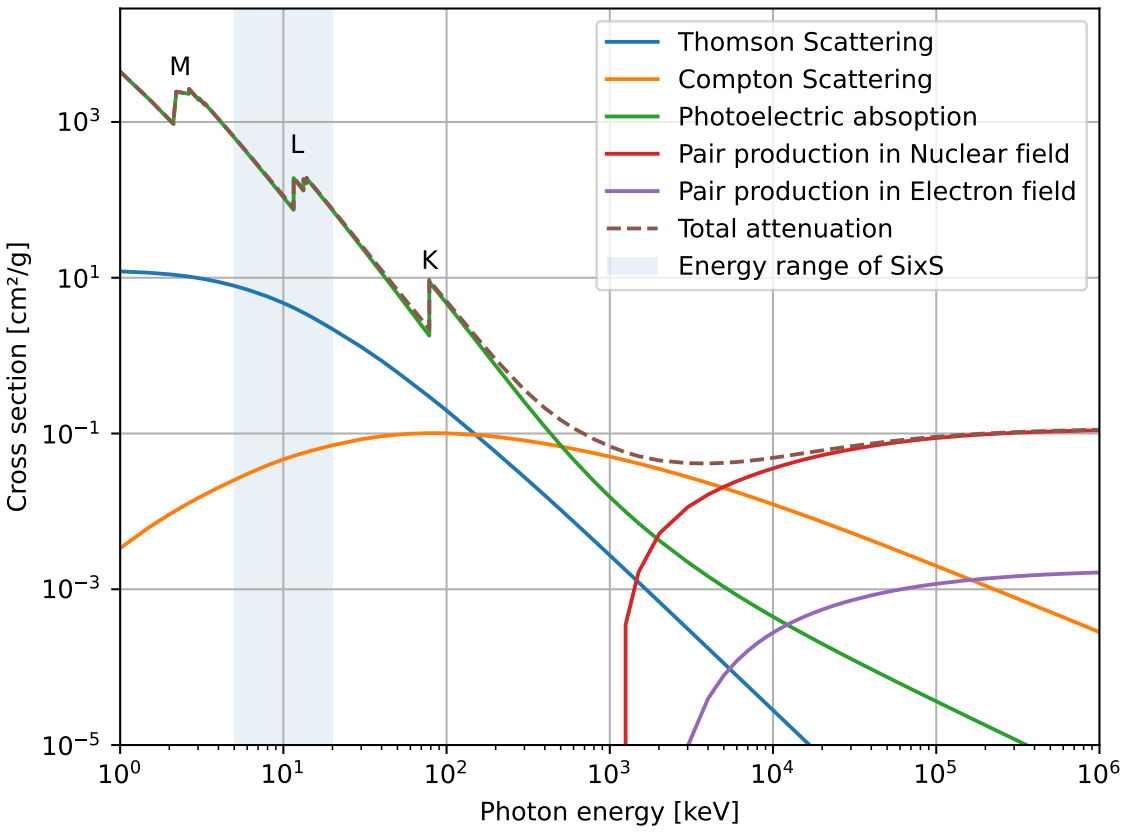

Figure 2.2: Cross-sections for Platinum (Z=78) for various processes that occur when photons interact with matter. The data was taken from the NIST (National Institute of Standards and Technology) (Berger et al. 2010) website. The energy range of the SixS beamline at SOLEIL is highlighted in blue.

$$\frac{\vec{E}_{scatt}(R,\,t)}{\vec{E}_{in}} = -r_0 \frac{e^{\vec{k}.\vec{R}}}{|\vec{R}|}|\hat{\epsilon}.\hat{\epsilon}'| \tag{2.4}$$

with $|\vec{R}|$ the distance at which the scattering is detected at the time t. r_0 is the Thomson scattering length defined as:

$$r_0 = \frac{e^2}{4\pi\epsilon_0 m_e c^2} \tag{2.5}$$

The minus sign illustrates a phase shift of π between the incident and scattered wave, $\hat{\epsilon}$ and $\hat{\epsilon}'$ are respectively the polarization vectors of the incident and scattered electromagnectic fields.

The differential cross-section for Thomson scattering measures the efficiency of the scattering in the volume occupied by a solid angle $d\Omega$ in the direction $\vec{R}$ (Jens Als-Nielsen 2011). It is defined as follows:

$$\frac{d\sigma_{ts}}{d\Omega} = \frac{|\vec{E}_{scatt}(R,t)|^2 R^2}{|\vec{E}_{in}|^2} \tag{2.6}$$

By substituting eq. 2.4 into eq. 2.6, it becomes clear that the scattering is proportional to the Thomson scattering length and that the intenisty is attenuated depending on the dot product between the two polarizations. The polarization factor P for scattered beams is defined as $P = |\hat{\epsilon}.\hat{\epsilon}'|^2$ and we can write the differential cross-section as:

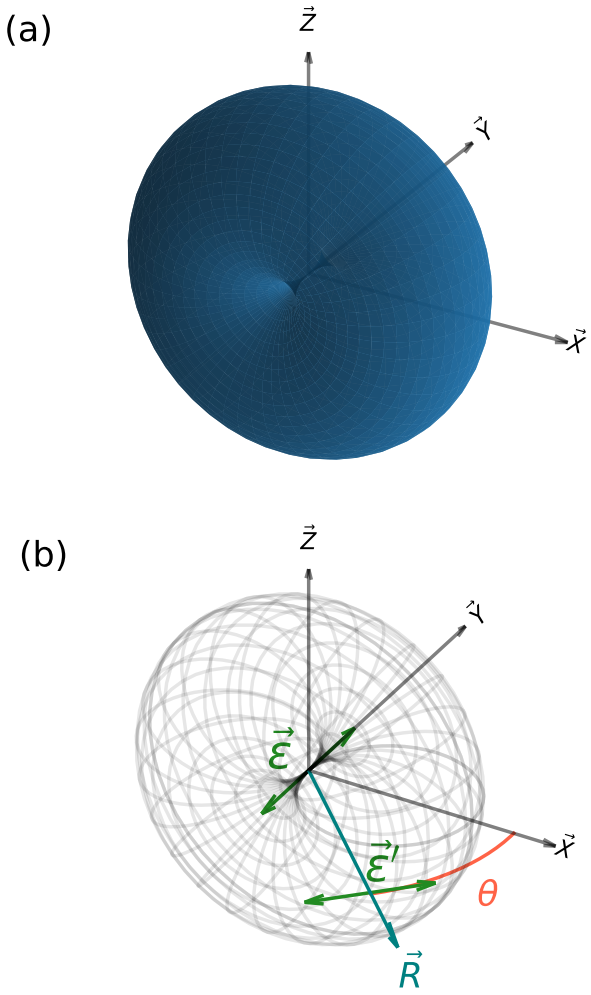

Figure 2.3: Effect of relation between synchrotron X-ray polarization $\hat{\epsilon}$ and scattered X-ray polarization $\hat{\epsilon}'$ on the scattered field. The scattered field intensity is attenuated by a $\cos\theta$ factor, where θ is the angle between the plane perpendicular to the electric field and the direction of observation $\vec{r}$. Working in the vertical plane is preferable to maximize the intensity of the scattered field, this has pratical repercussions in surface X-ray diffraction for which it is preferable to work in a vertical geometry to scan large 2D areas of the reciprocal space.

$$\frac{d\sigma_{ts}}{d\Omega} = r_0^2 |\hat{\epsilon}.\hat{\epsilon}'|^2 = r_0^2 P \tag{2.7}$$

The effect of the polarization of the incident beam is illustrated in figure 2.3. At synchrotron sources where the incident beam is horizontally polarized, working in the vertical plane becomes more effective since the polarization factor is always equal to one.

The total cross-section for the scattering event by a single free electron can be computed by integrating the differential cross-section over all the possible scattering angles, ie. by averaging

all possible polarization directions (Willmott 2009). This yields $\sigma_{ts} = 8\pi r_0^2/3 = 0.665\text{b}$, the total Thomson scattering cross-section is constant, independant of the incoming photon energy. This results holds for X-rays for which the scatterer i.e. the electron can be considered as free (Willmott 2009).

Scattering from a single atom

As we have seen the main scatterer for Thomson scattering is the electron. Each atom can be described as a small volume $d^3\vec{r}$ in the electronic density, and the scattered field by the superposition of the contribution from the electronic cloud surrounding the atoms.

The scattering of the incident beam from an atom is therefore proportional to the electronic density $\rho_{atom}(\vec{r})$. For a single atom of atomic number Z we have :

$$\int \rho_{atom}(\vec{r}) d^3\vec{r} = Z \tag{2.8}$$

The scattering amplitude shows a dependance depending on the wavelength of the incident beam λ, and on the direction of detection defined by the scattering angle 2θ between the wavevector of the incident photon $\vec{k_i}$ and the wavevector of the scattered photon $\vec{k_s}$ (fig. 2.4).

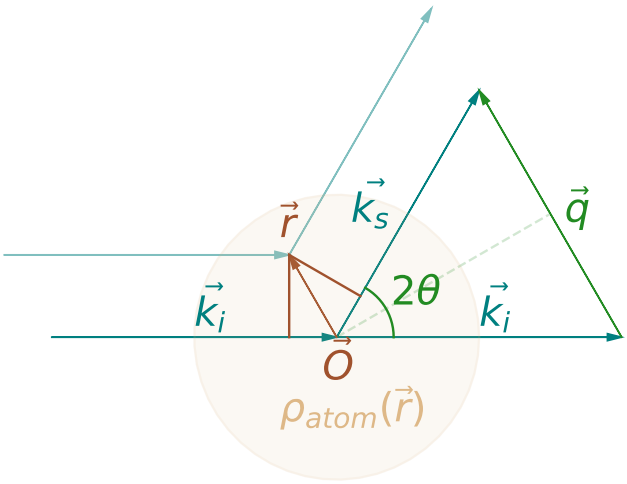

Figure 2.4: Geometry of the scattering vector $\vec{q}$ in reciprocal space, 2θ is the scattering angle. The magnitude of the scattering vector can be derived with the angle θ that draws a line cutting $\vec{q}$ at $|\vec{q}|/2$.

This leads to the definition of the scattering vector, $\vec{q}$, to describe the amplitude of a scattering event (eq. 2.9, fig. 2.4).

$$\vec{q} = \vec{k_i} - \vec{k_s} = 2|\vec{k}| \sin\theta \tag{2.9}$$

$$|\vec{q}| = \frac{4\pi}{\lambda} \sin\theta \tag{2.10}$$

The phase difference between a wave scattered at a position $\vec{O}$ and a wave scattered at a position $\vec{O} + \vec{r}$ is equal to $(\vec{k_i} - \vec{k_s}).\vec{r} = \vec{q}.\vec{r}$ (fig. 2.4). We assume here that the scattering event is elastic ($|\vec{k_i}| = |\vec{k_s}|$) and that the waves are plane waves parallel to each other when in the small scattering volume $d^3\vec{r}$.

A small volume $d^3\vec{r}$ will have a contribution equal to $-r_0\rho(\vec{r})d^3\vec{r}$ to the scattered field with a phase $e^{i\vec{q}.\vec{r}}$.

By integrating over the volume occupied by the atom we obtain the total contribution of an atom to the scattered field in the direction 2θ:

$$-r_0 \int \rho(\vec{r}) e^{i\vec{q}.\vec{r}} d\vec{r} = -r_0 f(\vec{q}) = -r_0 FT[\rho(\vec{r})] \tag{2.11}$$

The scattering amplitude as a function of $\vec{q}$ is described by the atomic scattering factor $f(\vec{q})$, which is defined as the Fourier transform of the electronic density $\rho(\vec{r})$. This hypothesis is at the basis of several techniques such as Bragg coherent diffraction imaging for which we use Fourier transforms to compute the scattered amplitude (sec. X).

The values for the atomic scattering factor can be calculated using tabulated coefficients (eq. 2.12) available online (Brown et al. 2006). It decreases with $\vec{q}$ (or $\sin(\theta)/\lambda$) as illustrated in figure 2.5.

$$f(\vec{q}) = \sum_{i=1}^{4} a_i \exp(-b_i(\frac{q}{4\pi})^2) + c \tag{2.12}$$

The scattering intensity is equal to the square of the scattering amplitude. For example, the scattering intensity of palladium atoms at $|\vec{q}| \approx 2.75$Å is only $\approx 31\%$ of that of platinum atoms. In the case of oxygen, the intensity falls down to $\approx 6.7\%$. This difference in scattering intensity between elements becomes crucial when working with small objects that have a small scattering volume such as nanoparticles, as in Bragg Coherent Diffraction Imaging.

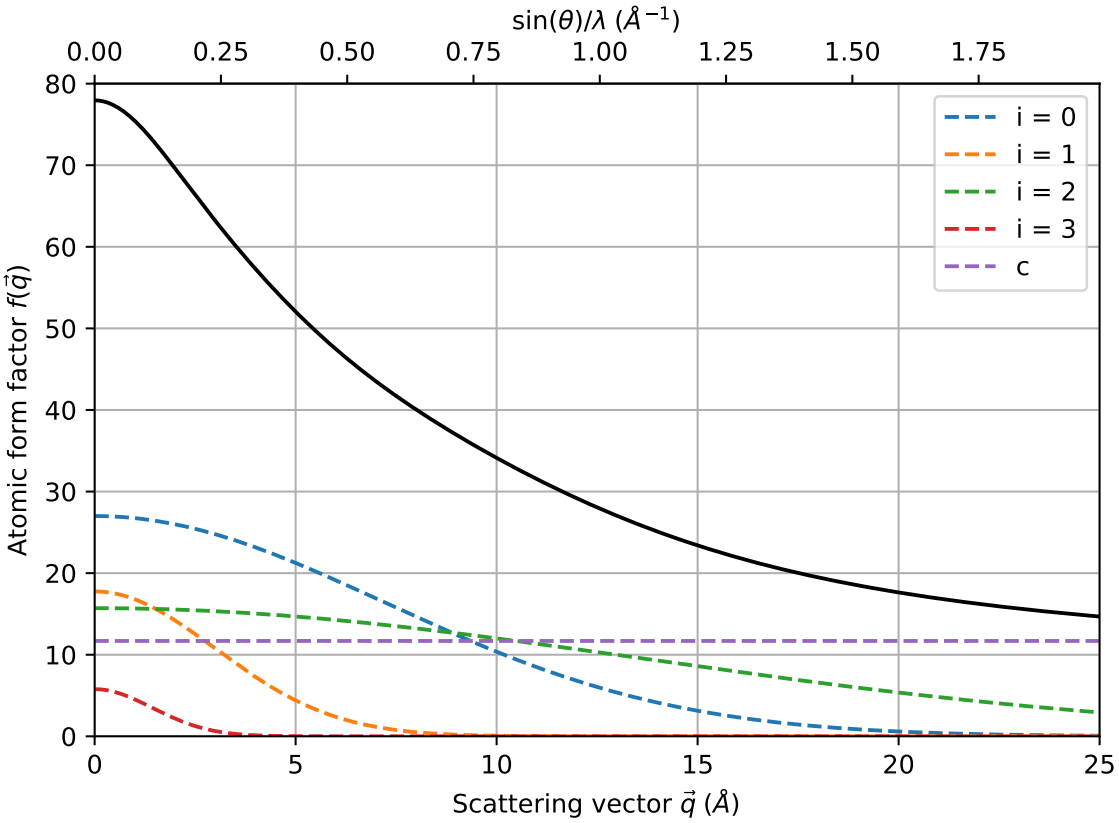

Figure 2.5: Atomic form factor calculated for Pt (Z=78) using tabulated values (Brown et al. 2006) for equation 2.11. The scattering intensity decreases with the scattering angle θ but increases with the incident wavelength λ. i and c respectively designate the Gaussian contribution and constant in eq. 2.12.

2.1.2 Scattering from crystals

A crystal is a solid material composed of a regular, repeating arrangement of atoms, ions, or molecules (i.e. a pattern), exhibiting a highly ordered structure with long-range periodicity in three dimensions.

A Bravais lattice refers to an infinite array of points (nodes) that represents the basic repeating unit of a crystal lattice, defining the translational symmetry of the crystal structure. It is characterized by a set of three basis vectors and their linear combinations, which generate the entire lattice when translated in space. The *primitive* unit cell is the smallest cell with which you can describe the crystal.

The structure of the Bravais lattice (cubic, hexagonal, ...) combined with the position of the patterns in the lattice and the symmetry relations between them defines the crystal *space group*. In total there exist 230 space group in crystallography. In the simplest case the pattern consists of a single atom, for example pure Platinum (Z=78) cristallizes at room temperature in a cubic Bravais lattice (fig. 2.6).

We can define the scattering factor $F_{crystal}$ of the crystal by the sum of the atomic scattering factor of each atom present in the crystal: why

$$F_{crystal} = \sum_{j}^{N_{atom}} f_j(\vec{q}) e^{i\vec{q}.\vec{r}_j} \tag{2.13}$$

$f_j(\vec{q})$ is the atomic scattering factor of the j-ieth atom at position $\vec{r}_j$ in a crystal made of N_{atom} atoms. The Thomson scattering length is left apart for simplicity.

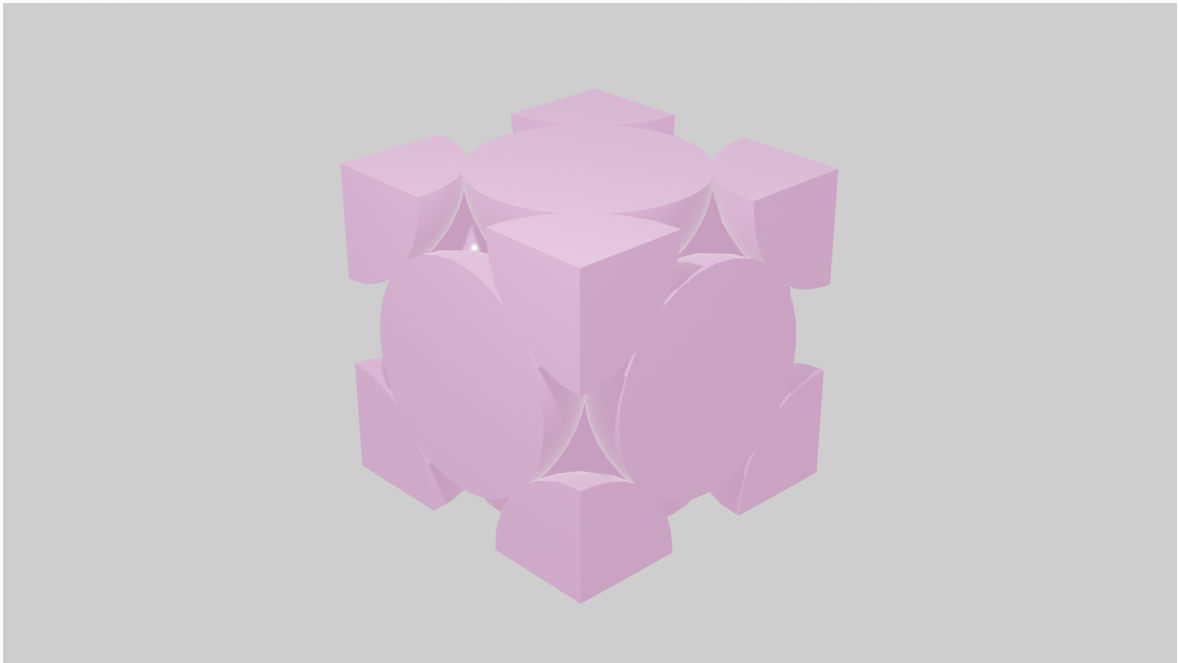

Figure 2.6: Face centered cubic (FCC) lattice of Pt (space group 225). Atoms are represented as solid balls and situated on the corners, at the middle of the faces, and at the center of the cube. The lattice parameter at room temperature is $\vec{a} = 3.9254$Å. Close packed direction is achieved along the diagonal of the lateral faces, thee distance between the atoms then becomes is 2.71Å.

The position of any atom in the crystal $\vec{r}_j$ is equal to the sum of the position of the unit cell $\vec{R}_{uc}$ plus the position of the atom within the unit cell $\vec{r}_j$. For a crystals made of N_{uc} unit cells each composed of N_{atoms} we have:

$$F_{crystal} = \sum_{j}^{N_{atoms}} f_j(\vec{q}) e^{i\vec{q}.\vec{r}_j} \sum_{k}^{N_{uc}} e^{i\vec{q}.\vec{R}_k} \tag{2.14}$$

The Bravais lattice is defined by three basis vectors $\vec{a}$, $\vec{b}$, $\vec{c}$ and three angles α $[\angle(\vec{b},\vec{c})]$, β $[\angle(\vec{a},\vec{c})]$ and γ $[\angle(\vec{a},\vec{b})]$. Any vector $\vec{R_k}$ describing the position of a node in the real space can be created by a linear combination of these three vectors:

$$\vec{R_k} = n_1\vec{a} + n_2\vec{b} + n_3\vec{c}, \qquad (n_1, n_2, n_3) \in \mathbb{Z}^3 \tag{2.15}$$

To understand the contribution of the second sum in eq. 2.14, it is convenient to introduce the *reciprocal space* which is the Fourier transform of the real space. It is defined by three basis vectors $\vec{a*}$, $\vec{b*}$, $\vec{c*}$. Similarly, the nodes of the reciprocal space can be accessed from its origin by a linear combination $\vec{G}$ of these three vectors.

$$\vec{a^*} = \frac{2\pi}{V}(\vec{b}\times\vec{c}), \qquad \vec{b^*} = \frac{2\pi}{V}(\vec{c}\times\vec{a}), \qquad \vec{c^*} = \frac{2\pi}{V}(\vec{a}\times\vec{b}), \qquad \vec{a}_i.\vec{a}_j^* = \delta_{i,j} \tag{2.16}$$

$$\vec{G} = h\vec{a^*} + k\vec{b^*} + l\vec{c^*}, \qquad (h,k,l) \in \mathbb{Z}^3 \tag{2.17}$$

By combining eq. 2.15 and eq. 2.17 we find that the solution to the equation $\vec{q}.\vec{R_k} = n\times 2\pi$ ($n \in \mathbb{Z}$) is to write $\vec{q}$ as a linear combination of the reciprocal space vectors, i.e. as $\vec{G}$.

$$\vec{G}.\vec{R_k} = hn_1 + kn_2 + ln_3 = n \quad with\ n \in \mathbb{Z} \tag{2.18}$$

This is also known as the Laue condition, that ensures that only certain scattering vectors, corresponding to the reciprocal lattice points, fulfill the condition for constructive interference between the scattered waves. These specific scattering vectors determine scattering direction and angle of the peaks observed in a diffraction pattern, also known as Bragg peaks.

$$\vec{q} = \vec{G} = h\vec{a^*} + k\vec{b^*} + l\vec{c^*} \tag{2.19}$$

2.1.3 Bragg's Law

The intensity scattered from a crystal as a function of the scattering vector $\vec{q}$ provides information about the arrangement and spacing of crystalline planes perpendicular to $\vec{q}$. The Miller indices are a set of integers used to represent the planes' orientation and spacing. A plane denoted by the (h,k,l) indices intercepts the axes $\vec{a}$, $\vec{b}$, $\vec{c}$ on the points $|\vec{a}|/h, |\vec{b}|/k, |\vec{c}|/l$. The direction perpendicular to the (hkl) plane is written as $[hkl]$, the distance between each plane is d_{hkl}.

A Bragg peak results from the constructive interference between coherently scattered waves at discrete values of the incident angle 2θ on a specific set of crystalline planes. From fig. 2.7 we can retrieve the condition to have constructive interference, also known as Bragg law and given by eq. (2.20).

$$n\lambda = 2d_{hkl}\sin\theta, \qquad n \in \mathbb{Z} \tag{2.20}$$

In the case of a cubic Bravais lattice, the distance between Miller planes can be written as:

$$d_{hkl} = \frac{2\pi}{|\vec{a^*}|\sqrt{h^2+k^2+l^2}} = \frac{|\vec{a}|}{\sqrt{h^2+k^2+l^2}} \tag{2.21}$$

From eq. 2.10, eq. 2.20 we fall back on the Laue condition which is a generalization of Bragg law. The diffraction order (n) in the Bragg's law equation can be omitted since it is implicitly determined by the Miller indices (hkl) representing the crystalline planes involved in the diffraction.

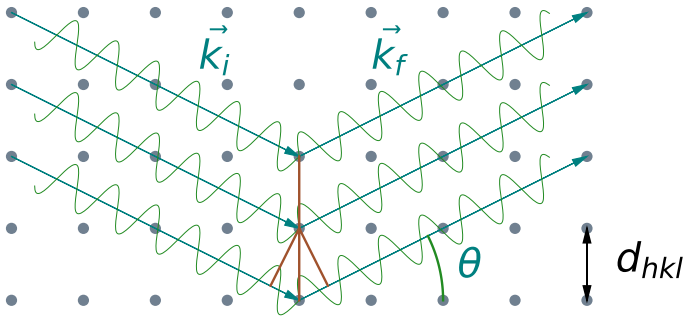

Figure 2.7: The difference in the path length between plane waves scattered at an angle θ must be an integer multiple of wavelengths for constructive interference to occur.

$$|\vec{Q}| = \frac{4\pi \sin(\theta)}{\lambda}, \tag{2.22}$$

$$\sin(\theta)/\lambda = \frac{1}{2d_{hkl}}, \tag{2.23}$$

$$|\vec{Q}| = \frac{2\pi}{d_{hkl}} \tag{2.24}$$

When fulfilling the Laue (or Bragg) condition, the direction of the scattering vector is perpendicular to the crystalline planes represented by the (h, k, l) Miller indices, and its magnitude is inversely proportional to the distance between consecutive crystalline planes.

2.1.4 Structure factor

On one hand, in real space, the crystal electronic density can be formed by repeating the unit cell at each lattice point, i.e. it can be represented as a convolution of the lattice and unit cell functions. This representation captures the periodicity and arrangement of the crystal.

On the other hand, in reciprocal space (Fourier space), the crystal scattering factor $F_{crystal}$ is the Fourier transform of the electronic density.why According to the convolution theorem, the Fourier transform of a convolution is equal to the product of the Fourier transforms of the individual functions. The scattering factor can therefore be expressed as the product of the Fourier transforms of the lattice and unit cell functions. These Fourier transforms are known as the lattice sum F_{lat} and the unit cell structure factor F_{uc}.

$$F_{crystal} = FT[\rho(\vec{r})] = F_{uc} * F_{lat} \tag{2.25}$$

The lattice sum F_{lat} represents the periodic arrangement of the crystal lattice in Fourier space, corresponding to the reciprocal lattice. It determines the positions and intensities of the diffraction peaks in the scattering pattern. The unit cell structure factor F_{uc} describes the distribution of electron density within the unit cell of the crystal and modulates the scattered beam amplitude depending on what atoms are in the unit cell (amplitude) and their positions (phase).

Each diffraction peak in the scattering pattern corresponds to a specific Fourier component, representing a sinusoidal wave of electron density with a particular frequency and direction determined by its position ((h, k, l) values) in Fourier space.

By knowing the phase relationships between these Fourier components, which can be obtained from the measured diffraction pattern, the electron density within the unit cell can be reconstructed. The superposition of these sinusoidal waves, representing the diffraction peaks or Fourier components, recreates the original electron density distribution of the crystal.

To summarize, the diffraction peaks in the scattering pattern represent the Fourier components of the crystal's electron density distribution, and their spatial frequencies and phase relationships carry information about the crystal structure.

By identifying the different parts of eq. 2.14 and eq. 2.25 we can first isolate the structure factor:

F_{hkl} is known as the structure factor, it is given by:

$$F_{uc} = \sum_{j}^{N_{atoms}} f_j(\vec{q}) e^{i\vec{q}.\vec{r}_j} \tag{2.26}$$

The structure factor is the summation of the contribution of each atom at the position $\vec{r}_j$ of atomic form factor $f(\vec{q})$ in the unit cell for a given $\vec{q}$. The position of the atom $\vec{r}_j$ is given by:

$$\vec{r}_j = x_j\vec{a} + y_j\vec{b} + z_j\vec{c} \tag{2.27}$$

2.1.5 Lattice factor

2.1.6 Coherence

So far we have limited ourselves to the kinematical approach of diffraction in the frame of this thesis. This means that multiple scattering and effect of absorption and refraction are ignored during diffraction. This is justified for Surface X-ray diffraction by the fact that the incoming angle is very low (≈ 0.3) and for BCDI by the low volume of the sample ($\approx 0.1\mu m^3$).

Field / amplitude / intensity consistent ? r_0 use consistent ? Where to mention that here we are using several hypothesis (Born approximation, DWBA, dipole), real crystals, fourier tranform, convolution

Bibliography

Resta, Andrea et al. (2020). 'Ammonia Oxidation over a Pt25Rh75(001) Model Catalyst Surface: An Operando Study'. In: *Journal of Physical Chemistry C* 124.40, pp. 22192–22199. ISSN: 19327455. DOI: 10.1021/acs.jpcc.0c07128.

Willmott, Philip (2009). *An Introduction to Synchrotron Radiation: Techniques and Applications*. John Wiley and Sons, Ltd. DOI: 10.1002/9781119280453.

Berger, M.J. et al. (2010). *NIST Standard Reference Database 8 (XGAM)*. DOI: https://dx.doi.org/10.18434/T48G6X. URL: https://www.nist.gov/pml/xcom-photon-cross-sections-database (visited on 15/06/2023).

Jens Als-Nielsen, Des McMorrow (2011). *Elements of Modern X-ray Physics*. John Wiley and Sons, Ltd. DOI: 10.1002/9781119998365.

Brown, P. J. et al. (2006). *International Tables for Crystallography*. Vol. C. Chap. 6.1, pp. 554–595. DOI: 10.1107/97809553602060000600.

université PARIS-SACLAY

ÉCOLE DOCTORALE
Physique en île de France
(PIF)

Titre: Propriétés catalytiques à l'échelle nanométrique sondées par diffraction des rayons X de surface et imagerie de diffraction cohérente
Mots clés: Diffraction, Catalyse, Surface, Structure, Déformation

Résumé: Le principal objectif est d'imager des nanostructures pour sonder les conditions in situ et operando ; mesurer la structure à l'échelle nanométrique et révéler également les effets de masse, de surface et d'interface ainsi que les défauts. Viser à terme à comprendre les phénomènes structurels importants pour les nanocatalyseurs et les relier à leur activité, sélectivité, réutilisabilité et durabilité. En complément des études cohérentes aux rayons X sur des particules individuelles, des techniques étudiants la moyenne des ensembles comme la diffraction des rayons X à incidence rasante seront employées pour voir si l'évolution des formes d'ensemble sont similaires à celles des nanoparticules uniques et sondent s'il y a une déconnexion entre les particules uniques et l'activité catalytique sur des billions de particules. La catalyse des nanomatériaux est apparue comme un moyen efficace d'exposer une surface plus élevée et d'accélérer les processus catalytiques en maximisant le rapport surface-volume. Le développement d'une catalyse hétérogène avec une sélectivité ciblant les 100% est un défi constant ainsi que la compréhension de la durabilité et du vieillissement du catalyseur lui-même. Dans un procédé réel (réacteur d'usine de catalyseur, échappement de voiture, pile à combustible), l'évolution de la forme et de la déformation des nanoparticules catalytiques dans des conditions de réaction contribue au vieillissement du catalyseur et a un impact sur la durée de vie du dispositif. Cependant, le processus catalytique et les changements structurels associés restent encore mal compris. Comprendre comment la structure du catalyseur est affectée par la couche adsorbée dans des conditions de réaction est donc de la plus haute importance pour formuler des relations de performance de structure de catalyseur qui guident la conception de meilleurs catalyseurs.

Title: Catalytic properties at the nanoscale probed by surface X-ray diffraction and coherent diffraction imaging
Keywords: Diffraction, Catalysis, Surface, Structure, Strain

Abstract: The main objective is to image nanostructures to probe in situ and operando conditions; measure the structure at nanoscale and to reveal bulk, surface and interface effects, as well as defects. Ultimately aiming to understand the structural phenomena important for the working nanocatalysts and link them to their activity, selectivity, reusability and sustainability. In complement to coherent x-ray studies on individual particles, ensemble-averaging techniques like grazing incidence x-ray diffraction will be employed to see if the evolution of ensemble shapes is similar to the one of single nanoparticles and probe if there is a disconnect between single particles and the catalytic activity over trillions of particles. Catalysis of nanomaterials has emerged as an efficient way to expose higher surface area and accelerate catalytic processes by maximizing the surface-volume ratio. The development of heterogeneous catalysis with selectivity targeting the 100% is a constant challenge as well as understanding the durability and ageing of the catalyst itself. In a real process (catalyst plant reactor, car exhaust, fuel cell) the shape and strain evolution of catalytic nanoparticles under reaction conditions contributes to the ageing of the catalyst and impact the lifetime of the device. However, the catalytic process and the associated structural changes remain poorly understood. Understanding how catalyst structure is affected by the adsorbed layer under reaction conditions is therefore of utmost importance to formulate catalyst structure performance relations that guide the design of better catalysts.

Maison du doctorat, Université Paris-Saclay
2e étage, aile ouest, École normale supérieure Paris-Saclay
4 avenue des Sciencs
91190 Gif-sur-Yvette, France